



Trans. Nonferrous Met. Soc. China 25(2015) 510-519

Transactions of Nonferrous Metals Society of China

www.tnmsc.cn



# Effect of preparation routes on activity of Ag–MnO<sub>x</sub>/C as electrocatalysts for oxygen reduction reaction in alkaline media

Qiu-mei WU<sup>1</sup>, Jian-ming RUAN<sup>1</sup>, Zhong-cheng ZHOU<sup>1</sup>, Shang-bin SANG<sup>2</sup>

- 1. State Key Laboratory of Powder Metallurgy, Central South University, Changsha 410083, China;
- 2. College of Chemistry and Chemical Engineering, Central South University, Changsha 410083, China

Received 21 March 2014; accepted 9 July 2014

**Abstract:** The effect of preparation routes on the physical characteristics and activity of the Ag–MnO<sub>x</sub>/C composites toward the oxygen reduction reaction (ORR) in alkaline media were studied by X-ray diffraction (XRD), X-ray photoelectron spectroscopy (XPS), transmission electron microscopy (TEM), energy-dispersion spectroscopy (EDS) as well as scanning electron microscopy (SEM) and electrochemical techniques. The results show that more Ag and Mn species present on the surface of the Ag–MnO<sub>x</sub>/C composite prepared by two-step route (Ag–MnO<sub>x</sub>/C-2) compared to the one prepared by one-step route (Ag–MnO<sub>x</sub>/C-1), which contributes to its superior activity toward the ORR. The higher electron transfer number involved in the ORR can be observed on the Ag–MnO<sub>x</sub>/C-2 composite and its specific mass kinetic current at –0.6 V (vs Hg/HgO) is 46 mA/μg, which is 23 times that on the Ag/C. The peak power density of zinc–air battery with the Ag–MnO<sub>x</sub>/C-2 air electrode reaches up to 117 mW/cm<sup>2</sup>.

Key words: silver; manganese oxide; oxygen reduction reaction; zinc-air battery; electrocatalyst; full cell

# 1 Introduction

Oxygen reduction reaction (ORR), as the main cathode reaction of fuel cells and metal-air batteries, involves multiple electrons transfer, and its slow kinetics brings about the main voltage drop. At present, the widely used catalysts are still Pt-based catalysts due to their relatively high activity and stability [1]. However, the scarity and high cost of Pt hinder their large-scale application. The inherently faster kinetics of the ORR and the less corrosive environment to the catalysts and electrodes in alkaline environment than those in acid media make the possibility to replace Pt-based catalysts with the less costly non-platinum electrocatalysts, such as Pd [2,3], Fe-N-C [4] in recent years. Among these numerous candidates, silver, as the less expensive noble metal, is considered one of the top substitutes for Pt in alkaline media due to its relatively high activity toward the ORR, excellent short term stability as well as the methanol tolerant ability [5–7].

The recent researches about Ag as the ORR catalyst mainly focused on the effects of the morphology [8], metal loading [5], particle size [9] and protecting ligand [10] on the ORR activity. However, compared with the

Pt-based catalysts, the activity of Ag toward the ORR is still not satisfied due to the poor affinity between Ag and O<sub>2</sub>, which leads to the difficulty in breaking O—O bond [11]. In order to further increase the activity, some carbon supported Ag hydrids or alloys have been prepared, such as Ag-MnO<sub>x</sub>/C [12,13], AgPt [14], AgPd [15]. Among these catalysts, the less expensive Ag-MnO<sub>x</sub>/C hybrids have been concerned because a synergistic effect among Ag and MnO<sub>x</sub> may exist, which accounts for the improved ORR activity [16].

As well known, the ORR activity of catalyst is greatly affected by material's surface property rather than its bulk property. So a controlled method which is easier to adjust the content of active species on the catalyst surface should be considered. In the present work, a method was introduced to prepare the  $Ag-MnO_x/C$  catalyst with more active materials on its surface, and the physical characteristics as well as the activity of the composites toward the ORR were studied and compared with those of the 30% Ag/C.

# 2 Experimental

#### 2.1 Chemicals and materials

The Vulcan<sup>@</sup> XC-72 was purchased from Cabot

Company. KMnO<sub>4</sub>, NaBH<sub>4</sub> and AgNO<sub>3</sub> were obtained from Tianjin Damao Chemical Reagent Factory and sodium citrate was purchased from Tianjin Bodi Chemical Holding Co., Ltd., China. All these chemicals are of analytic reagent grade and used as received.

#### 2.2 Synthesis of electrocatalysts

The Ag-MnO $_x$ /C composites with the Ag and MnO $_x$ (MnO<sub>2</sub> counted as the active material) mass loadings of 10% and 20%, respectively, were prepared by one-step and two-step routes. For the two-step route, 145.4 mg KMnO<sub>4</sub> was added into the homogeneous aqueous suspension of carbon black (288 mg XC-72, 92 mL H<sub>2</sub>O). The mixture was stirred at 80 °C for 30 min after the KMnO<sub>4</sub> was dissolved thoroughly, then AgNO<sub>3</sub> aqueous solution (63 mg AgNO<sub>3</sub>, 10 mL H<sub>2</sub>O) was poured into the suspension, followed by stirring for another 30 min at 80 °C. The resultant precipitate was filtrated, washed by deionized water, and dried at 70 °C in vacuum. The sample prepared by this method was denoted as Ag-MnO<sub>x</sub>/C-2. For the sample prepared by one-step route and denoted as Ag-MnO<sub>x</sub>/C-1, the process was the same as that for Ag-MnO<sub>x</sub>/C-2 catalyst except the KMnO<sub>4</sub> and AgNO<sub>3</sub> were added into the carbon aqueous suspension simultaneously. The results of X-ray fluorescence (XRF) examinations for all the filtrates show the complete deposition of silver and manganese onto the carbon support. For comparison, the 30% MnO<sub>x</sub>/C composite was synthesized as follows: the homogeneous aqueous suspension of 146 mg carbon and 109 mg KMnO<sub>4</sub> was stirred vigorously for 30 min at 80 °C, then filtrated, washed, and dried at 70 °C in vacuum. On the other hand, the 30% Ag/C was also synthesized according to Ref. [5].

# 2.3 Physical characterization

The crystalline structures of the catalysts were analyzed by X-ray diffraction (XRD) on a Rigaku X-2000 diffractometer using Cu  $K_{\alpha}$  radiation with a Ni filter. The morphologies of the composites were observed by transmission electron microscopy (TEM) operated on JEOL JEM-2011EM microscope and scanning electron microscopy (SEM) performed on QUANTA FEG250 microscope equipped with an energy-dispersion X-ray spectrometer. The element valences on the surface of the composites were analyzed by X-ray photoelectron spectroscopy (XPS) performed on Thermo Fisher Scientific K-Alpha (UK) using an Al  $K_{\alpha}$  radiation (1486.6 eV).

# 2.4 Electrochemical measurements

The activity and selectivity of the  $Ag-MnO_x/C$  composites toward the ORR were evaluated by the rotate disk electrode (RDE) and rotating ring-disk electrode

(RRDE) techniques in N<sub>2</sub> or O<sub>2</sub>-saturated 0.1 mol/L NaOH aqueous according to Ref. [17]. The RDE and RRDE tests were carried out on CHI 760D electrochemical workstation (Chenhua Company, China) and computer- controlled bipotentiostat (Pine Company), respectively. A glassy carbon disk electrode covered with a catalyst film was served as the working electrode. while Pt-wire and Hg/HgO electrodes were used as the counter and the reference electrodes, respectively. The working electrode was prepared as follows. 5.0 mg catalyst was mixed with 2 mL absolute ethanol and 40 μL Nafion solution (5%, mass fraction, DuPont), then formed a homogeneous ink ultrasonically. 20 µL of the prepared catalyst ink was deposited on the RDE or the disk of the RRDE, and then the solvent evaporated at room temperature. Besides, for the RRDE measurements, the ring potential was fixed at 0.20 V (vs Hg/HgO), high enough to oxidize the HO<sub>2</sub><sup>-</sup> produced on the working electrode. The  $HO_2^-$  productions (X( $HO_2^-$ )) and the electron transfer numbers (n) involved in the ORR calculated from the equations  $X(HO_2^-)=$  $(2I_{\text{ring}}/N)/(I_{\text{disk}}+I_{\text{ring}}/N)$  (N=0.38) and  $n=4-2X(\text{HO}_2^-)$ . All the potentials in this work refer to the Hg/HgO in 0.1 mol/L NaOH aqueous solution.

# 2.5 Performance tests of zinc-air batteries

In order to evaluate the performance of the composites in the actual working conditions, a homemade zinc-air single battery was fabricated with the air electrode and the zinc foil used as the cathode and anode, respectively, and the electrolyte was the 7 mol/L KOH aqueous solution. The 32 cm $^2$  (4 cm  $\times$  8 cm) air electrodes with different catalysts were prepared as follows. A certain amount of acetylene black, activated carbon, catalyst as well as 40% poly (tetrafluoroethylene) (PTFE) and deionized water were mixed and stirred mechanically to form homogeneous slurry. The certain amount of the slurry was brushed onto the Ni-foam with the back covered with gas diffusion layer, then the air electrodes were calcined at 200 °C in N2. The I-V discharge curves were recorded on the multichannel battery testing system (Neware Company).

#### 3 Results and discussion

#### 3.1 Physical characterization of composites

XRD patterns for the  $MnO_x/C$  and  $Ag-MnO_x/C$  composites are shown in Fig. 1. For comparison, the standard patterns for  $MnO_2(PDF 30-0820)$ ,  $Mn_3O_4(PDF 80-0382)$  and  $Ag_2O(PDF 12-0793)$  are included in the bottom of Fig. 1. For all the composites, the broadened peaks located at about  $2\theta$ =25.0° are assigned to graphite (002) of the carbon support. Besides, for the  $MnO_x/C$ , the

broadened peaks located at about  $2\theta$ =36.8° and 66.2° are attributed to  $\gamma$ -MnO<sub>2</sub> (100) and (110), respectively. While for the Ag–MnO<sub>x</sub>/C-1 sample, the diffraction peak positions and relative intensities are similar to those for the MnO<sub>x</sub>/C except for the broadened peak located at the range from 28° to 34° which may be attributed to Mn<sub>3</sub>O<sub>4</sub>, and no obvious peaks for silver species can be observed, which means that the silver species are either in amorphous or in very small particle size. However, for the Ag–MnO<sub>x</sub>/C-2 sample, the peaks located at about  $2\theta$ =28.9°, 32.4°, 36.0° and 59.9° are assigned to Mn<sub>3</sub>O<sub>4</sub> (112), (103), (211) and (224), respectively. Besides, the peaks located at about  $2\theta$ =32.4° and 37.1° may be overlapped with the Ag<sub>2</sub>O (111) and MnO<sub>2</sub> (100), respectively.

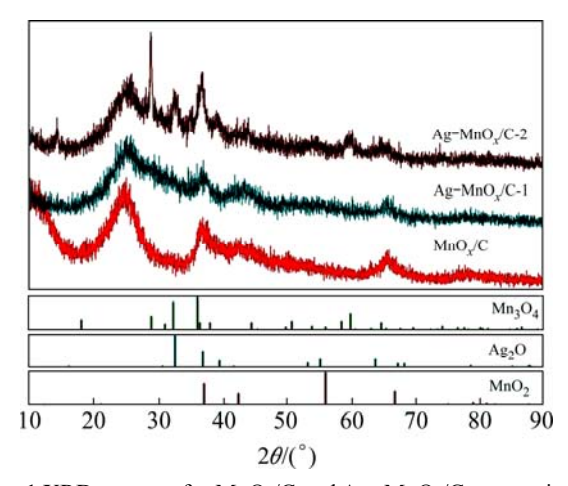


Fig. 1 XRD patterns for MnO<sub>x</sub>/C and Ag-MnO<sub>x</sub>/C composites

SEM images of the Ag-MnO<sub>x</sub>/C composites are shown in Figs. 2(a) and (b). It can be observed that the white and the relatively black regions for both samples can be distinguished. In order to further determine the different regions, the EDS experiments were performed and the results are also shown in Fig. 2. It is clear that Ag and Mn species mainly present on the white regions. The Mn and Ag contents on the Ag-MnO<sub>x</sub>/C-2 composite, averaged from the five points presented in Fig. 2(b), are 15.46% and 13.05% (mass fraction), higher than 13.31% and 10.00% for the Ag-MnO<sub>x</sub>/C-1, respectively. The corresponding atomic ratio of the x(Ag)/x(Mn) on the surface of Ag-MnO<sub>x</sub>/C-2 is 0.43, much higher than that (0.38) on the Ag-MnO<sub>x</sub>/C-1. It should be pointed out that the amounts of KMnO<sub>4</sub> and AgNO<sub>3</sub> used in the experiments are equal and the x(Ag)/x(Mn) atomic ratio is 0.40 combined with the results of XRF for the filtrates. Thus, it can be concluded that some Ag species for the Ag-MnO<sub>y</sub>/C-1 sample are agglomerated or coated by the carbon, while more Ag species present on the  $Ag-MnO_x/C-2$  surface.

The Ag  $3d_{5/2}$  and Mn  $2p_{3/2}$  XPS spectra for the Ag-MnO<sub>x</sub>/C composites are presented in Fig. 3.

According to Ref. [18], the Ag  $3d_{5/2}$  peak can be separated into two peaks at about 368.20 and 368.50 eV, corresponding to Ag<sub>2</sub>O and Ag(0), respectively, and the corresponding peak area percentages of each silver species are shown in Table 1. For the Ag-MnO<sub>x</sub>/C-1, a sharp peak without any additional peak shoulder suggests that there is very little other silver species and the main silver species is Ag<sub>2</sub>O, while for the Ag-MnO<sub>x</sub>/C-2 composite, the content of Ag(0) reaches 12.42%. For the Mn 2p<sub>3/2</sub> XPS, taking the shake-up peak into account, the peak can be separated into three peaks at about 640.89, 642.20 and 643.12 eV, corresponding to the Mn(II), Mn(III) and Mn(IV) [19], respectively, and the corresponding peak area percentages of each Mn species are also shown in Table 1. The percentages of each Mn species are comparable, i.e., the preparation routes have no obvious effect on the valent state of Mn.

The morphologies of the Ag-MnO<sub>x</sub>/C composites are observed through TEM and the results are shown in Fig. 4. The nano-spheres with the diameter of about 30 nm for both composites are carbon supports. For the Ag-MnO<sub>x</sub>/C-1 composite, some nano-sticks and a few floccules (blue arrows) present which may be attributed to the MnO<sub>x</sub> species. Besides, some nano-particles with the diameter of 7–8 nm (red cycles) present on the sticks which should be assigned to the Ag<sub>2</sub>O particles according to the XPS results. While for the Ag-MnO<sub>x</sub>/C-2 composite, few nano-sticks and nano-particles present, but more floccules appear. However, it is hard to discriminate the silver species and MnO<sub>x</sub> due to the low contrast between them.

# 3.2 Electrochemical characteristics of composites

Figure 5 shows the cyclic voltammetry (CV) curves in 0.1 mol/L N2-saturated NaOH solution for the Ag-MnO<sub>y</sub>/C composites with the scanning rate of 0.01 V/s after the fast scanning (0.10 V/s, 20 cycles) between -0.80 V and 0.40 V for the surface cleaning. It can be observed that in all the potential range, the positions of the redox peaks in the CVs for both Ag-MnO<sub>x</sub>/C composites are comparable. In the positive direction, according to Ref. [20], the anodic peaks located at about -0.25, -0.10 and 0.05 V could be attributed to the reactions of  $Mn(II) \rightarrow Mn_2O_3$ , Mn(II)→MnOOH and Mn(III)→Mn(IV), respectively. Further increasing the potential to 0.400 V, the anodic peaks in the range of 0.200 and 0.400 V are mainly assigned to the oxidation of Ag species [5]. In the negative direction, the peaks located at about 0.10 and -0.05 V are attributed to the reduction of the silver oxides to metallic silver and MnO<sub>2</sub> to MnOOH [5,20], respectively. When the potential goes negatively to the range of about -0.20 to -0.70 V, the reduction current for the Mn(III) to Mn<sub>3</sub>O<sub>4</sub> and Mn(OH)<sub>2</sub> is observed [20].

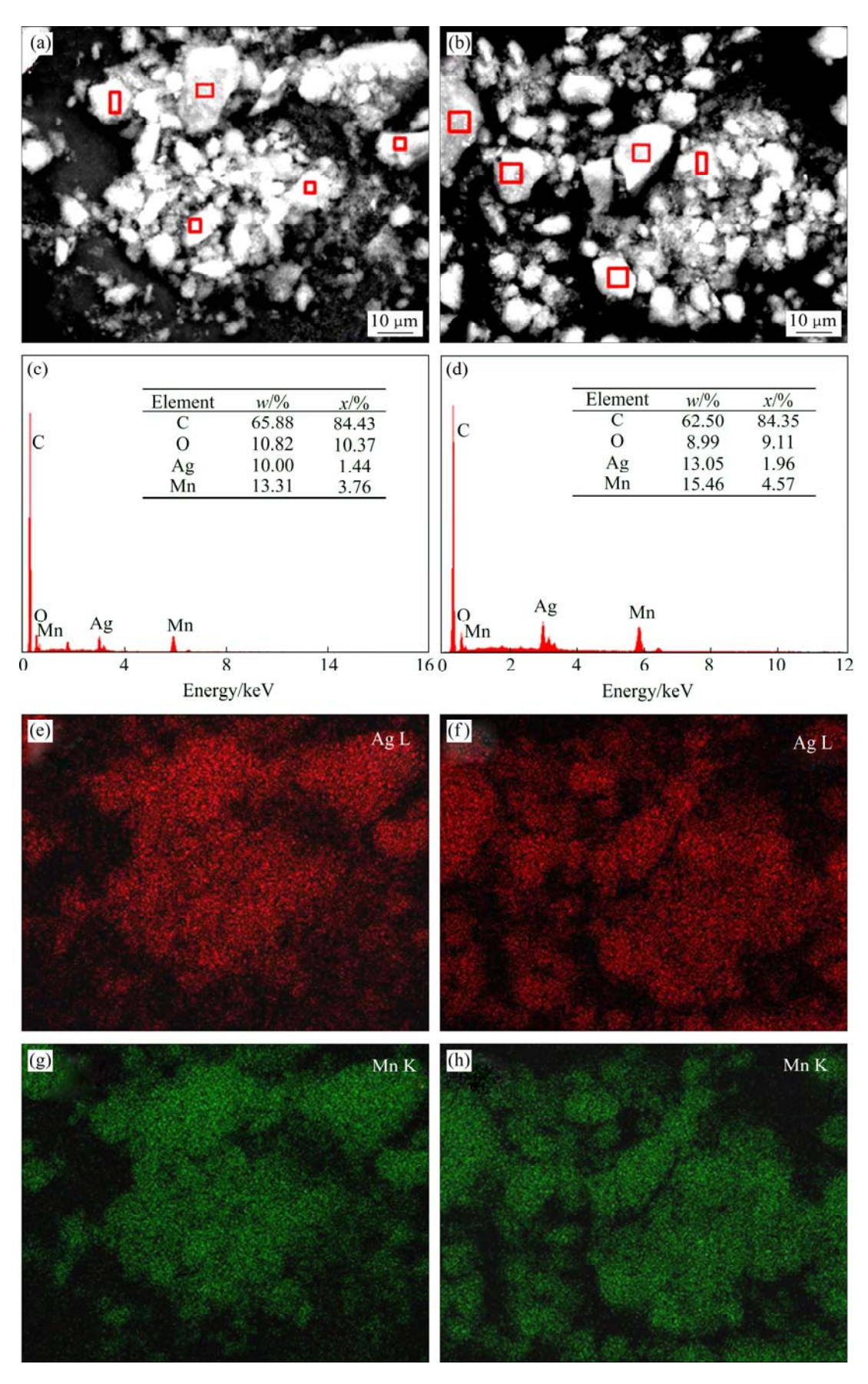
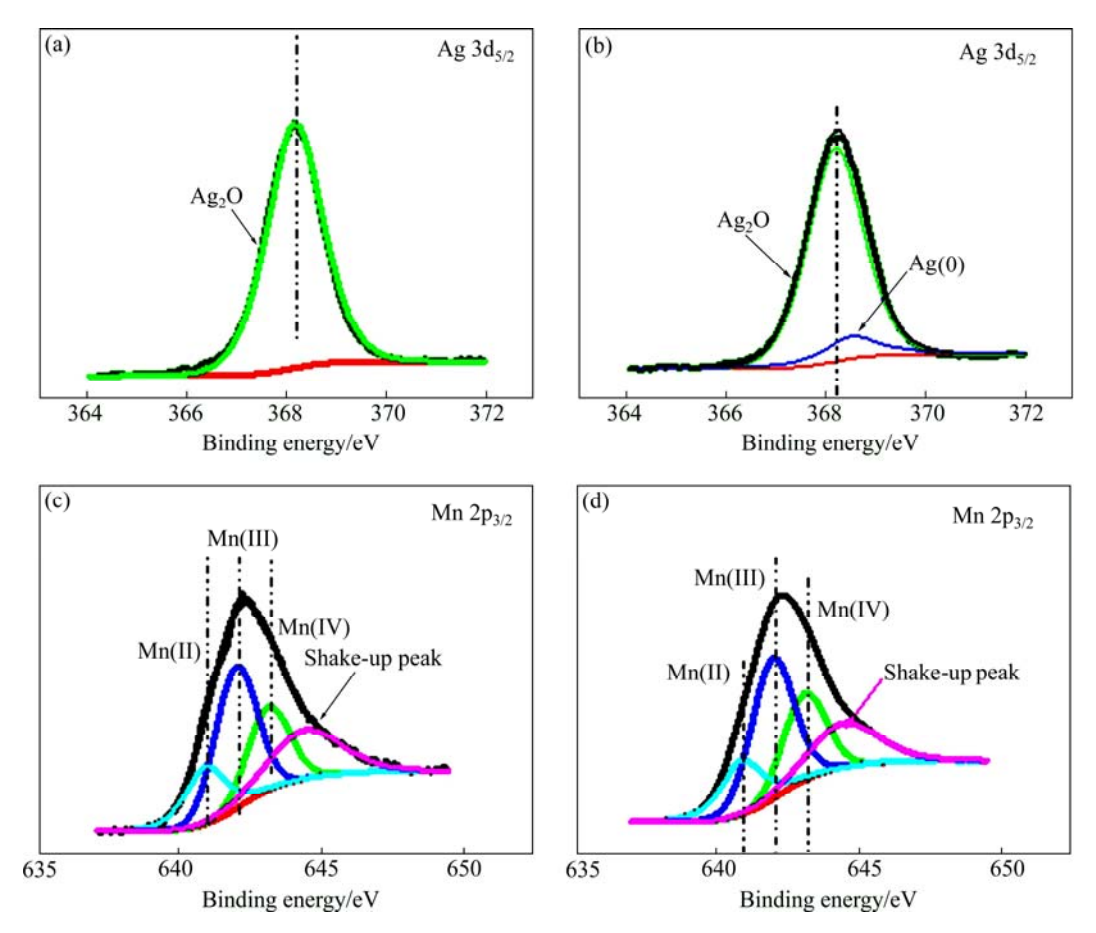


**Fig. 2** SEM images (a, b), EDS spectra (c, d), distribution mappings of Ag (e, f) and Mn (g, h) for Ag–MnO $_x$ /C-1 and Ag–MnO $_x$ /C-2: (a, c, e, g) Ag–MnO $_x$ /C-1; (b, d, f, g) Ag–MnO $_x$ /C-2



 $\textbf{Fig. 3} \ \text{XPS spectra of Ag 3d}_{5/2} \ \text{and Mn 2p}_{3/2} \ \text{for Ag-MnO}_x/C \ \text{composites: (a, c) Ag-MnO}_x/C-1; \ (b), \ (d) \ \text{Ag-MnO}_x/C-2 \ \text{Composites: (a, c) Ag-MnO}_x/C-1; \ (b), \ (d) \ \text{Ag-MnO}_x/C-2 \ \text{Composites: (a, c) Ag-MnO}_x/C-1; \ (b), \ (d) \ \text{Ag-MnO}_x/C-2 \ \text{Composites: (a, c) Ag-MnO}_x/C-1; \ (b), \ (d) \ \text{Ag-MnO}_x/C-2 \ \text{Composites: (a, c) Ag-MnO}_x/C-1; \ (b), \ (d) \ \text{Ag-MnO}_x/C-2 \ \text{Composites: (a, c) Ag-MnO}_x/C-1; \ (b), \ (d) \ \text{Ag-MnO}_x/C-2 \ \text{Composites: (a, c) Ag-MnO}_x/C-1; \ (b), \ (d) \ \text{Ag-MnO}_x/C-2 \ \text{Composites: (a, c) Ag-MnO}_x/C-1; \ (b), \ (d) \ \text{Ag-MnO}_x/C-2 \ \text{Composites: (a, c) Ag-MnO}_x/C-1; \ (b), \ (d) \ \text{Ag-MnO}_x/C-2 \ \text{Composites: (a, c) Ag-MnO}_x/C-1; \ (b), \ (d) \ \text{Ag-MnO}_x/C-2 \ \text{Composites: (a, c) Ag-MnO}_x/C-2 \ \text{Composite$ 

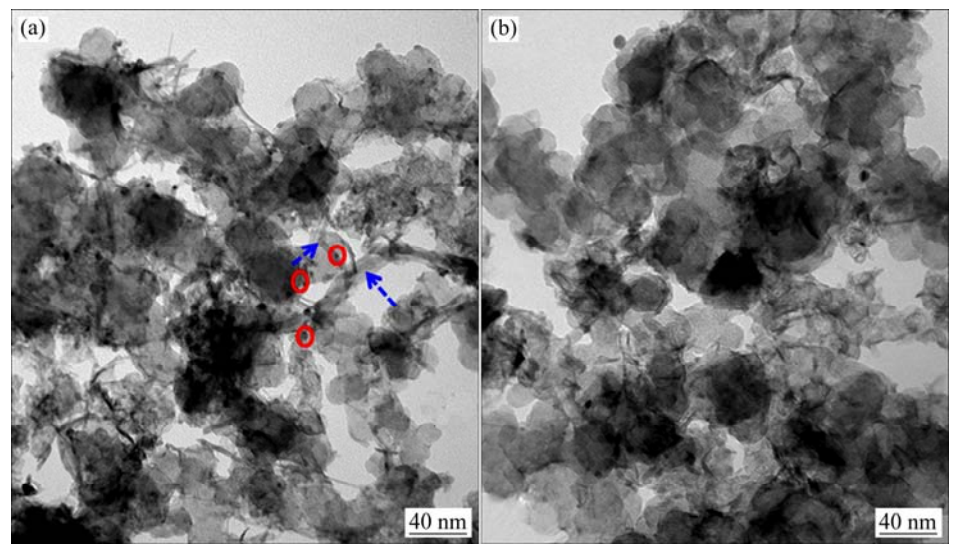
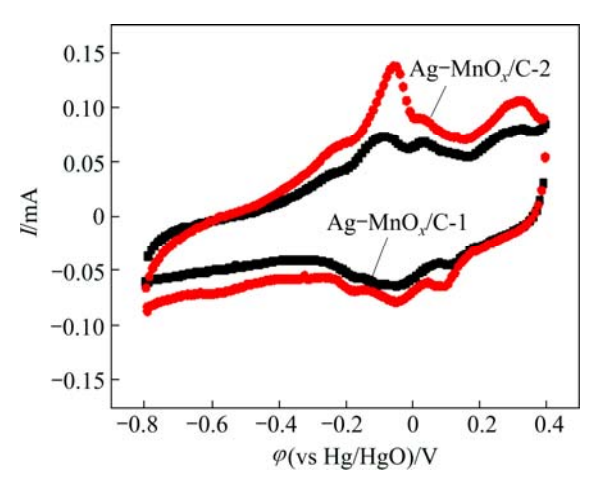


Fig. 4 TEM images for Ag-MnO<sub>x</sub>/C-1 (a) and Ag-MnO<sub>x</sub>/C-2 (b) samples

Table 1 Binding energy and chemical state of Ag  $3d_{5/2}$  and Mn  $2p_{3/2}$ 

Composite	Ag(0)		Ag(I)		Mn(II)		Mn(III)		Mn(IV)	
	Binding energy/eV	ratio/%								
Ag-MnO <sub>x</sub> /C-2	368.50	12.42	368.18	87.58	640.90	20.33	642.10	49.63	643.10	30.03
Ag-MnO <sub>x</sub> /C-1	368.50	0	368.20	100	640.89	21.00	641.99	49.76	643.12	29.24



**Fig. 5** CV curves for  $Ag-MnO_x/C$  composites in  $N_2$ -saturated 0.1 mol/L NaOH solution

It can be observed that the peaks areas associated with the oxidation of Mn(II) to MnOOH and the silver species oxidation for the Ag–MnO $_x$ /C-2 sample are much higher than those for the Ag–MnO $_x$ /C-1 composite, which may be due to the higher Mn and Ag contents on the surface of Ag–MnO $_x$ /C-2 according to the EDS analysis. On the other hand, the relatively low atomic ratio of  $x(Ag_2O)/x(Ag)$  on the surface of Ag–MnO $_x$ /C-2 can also contribute to the higher oxidation current for silver species with the XPS results combined.

# 3.3 Activity of Ag-MnO<sub>x</sub>/C composites toward ORR

To investigate the activity of the Ag-MnO<sub>x</sub>/C composites toward the ORR, linear voltammetry (LSV) measurements were performed on the catalyst film covered RDE in O2-saturated 0.1 mol/L NaOH solution with a rotation rate of 1600 r/min, as shown in Fig. 6. For comparison, the polarization curve for the 30% Ag/C is also presented. Though the onset potentials for the ORR on both Ag-MnO<sub>x</sub>/C samples are comparable (-0.051 V), about 0.019 V more positive than that on Ag/C. The half-wave potential ( $\varphi_{1/2}$ ) of the ORR on the Ag-MnO $_x$ /C-2 composite is -0.164 V, about 0.033 V and 0.058 V more positive than those on the Ag-MnO<sub>x</sub>/C-1 and Ag/C, respectively, and the limiting current ( $I_{lim}$ ) of the ORR on the Ag-MnO<sub>x</sub>/C-2 composite is also slightly higher than those observed on the Ag-MnO<sub>x</sub>/C-1 and Ag/C. According to Ref. [17], the ORR activities of MnO<sub>x</sub>/C and Ag/C are associated with the concentration of the Mn(III) on the surface and the surface area of Ag, respectively. According to the analysis of the EDS and the CVs, the higher ORR activity on the Ag-MnO<sub>x</sub>/C-2 than that on Ag-MnO<sub>x</sub>/ C-1 may be attributed to more Mn(III) and Ag species on its surface.

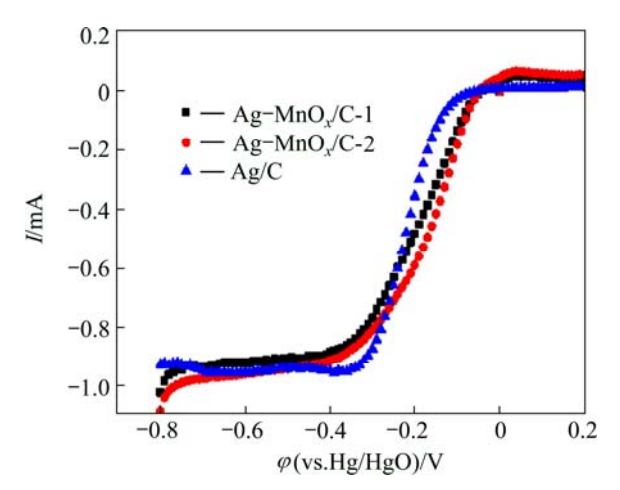


**Fig. 6** LSV curves for Ag–MnO<sub>x</sub>/C and Ag/C composites in O<sub>2</sub>-saturated 0.1 mol/L NaOH solution (Scanning rate: 0.01 V/s; rotation rate: 1600 r/min; electrode area: 0.196 cm<sup>2</sup>)

#### 3.4 ORR selectivity on Ag-MnO<sub>x</sub>/C composites

As well known, the ORR is a multi-electron transfer reaction which involves two main possible pathways: one is the  $2e^-$  pathways with the product being  $HO_2^-$  in alkaline media, and the other involves the  $4e^-$  pathways with the final product being  $H_2O$  [21]. The electron transfer numbers involved in the ORR can be calculated from the slope of the Koutecky-Levich (K-L) curves by plotting  $\Gamma^1$  versus  $\omega^{-1/2}$ . The K-L equation can be expressed as [22]

$$\frac{1}{I} = \frac{1}{I_{\rm k}} - \frac{1}{I_{\rm d}} = \frac{1}{nFAkc_{\rm O}} - \frac{1}{0.62nFAD^{2/3}\gamma^{-1/6}c_{\rm O}\omega^{1/2}} \ (1)$$

where I,  $I_k$  and  $I_d$  correspond to the measured, kinetic and diffusion limiting currents, respectively; n is the overall electron transfer number; F is the Faraday constant (96500 C/mol); D is the O<sub>2</sub> diffusion coefficient in 0.1 mol/L NaOH  $(1.9\times10^{-5} \text{ cm}^2/\text{s})$ ; A is the geometric electrode area (cm $^2$ ); k is the rate constant for oxygen reduction;  $\gamma$  is the kinematic viscosity (0.01 cm<sup>2</sup>/s);  $c_0$  is the oxygen concentration  $(1.2 \times 10^{-6} \text{ mol/cm}^3)$  [16]. The LSV curves recorded at different rotation rates and the K-L plots for the catalysts (just for the diffusion controlled region  $\varphi = -0.60 \text{ V}$ ) are shown in Fig. 7. With the rotating speed increasing, the  $I_{lim}$  of the ORR increases, while the ORR onset potential is kept almost unchanged. The electron transfer numbers calculated for the Ag/C, Ag-MnO<sub>x</sub>/C-1 and Ag-MnO<sub>x</sub>/C-2 are 3.93, 3.89 and 4.02, respectively. Though these values are all close to four, which indicates that the overall ORR process is an apparent 4e pathway, the value for the sample Ag-MnO<sub>x</sub>/C-2 is still slightly higher than those for Ag-MnO<sub>y</sub>/C-1 and Ag/C, which means that less  $HO_2^-$  is produced.

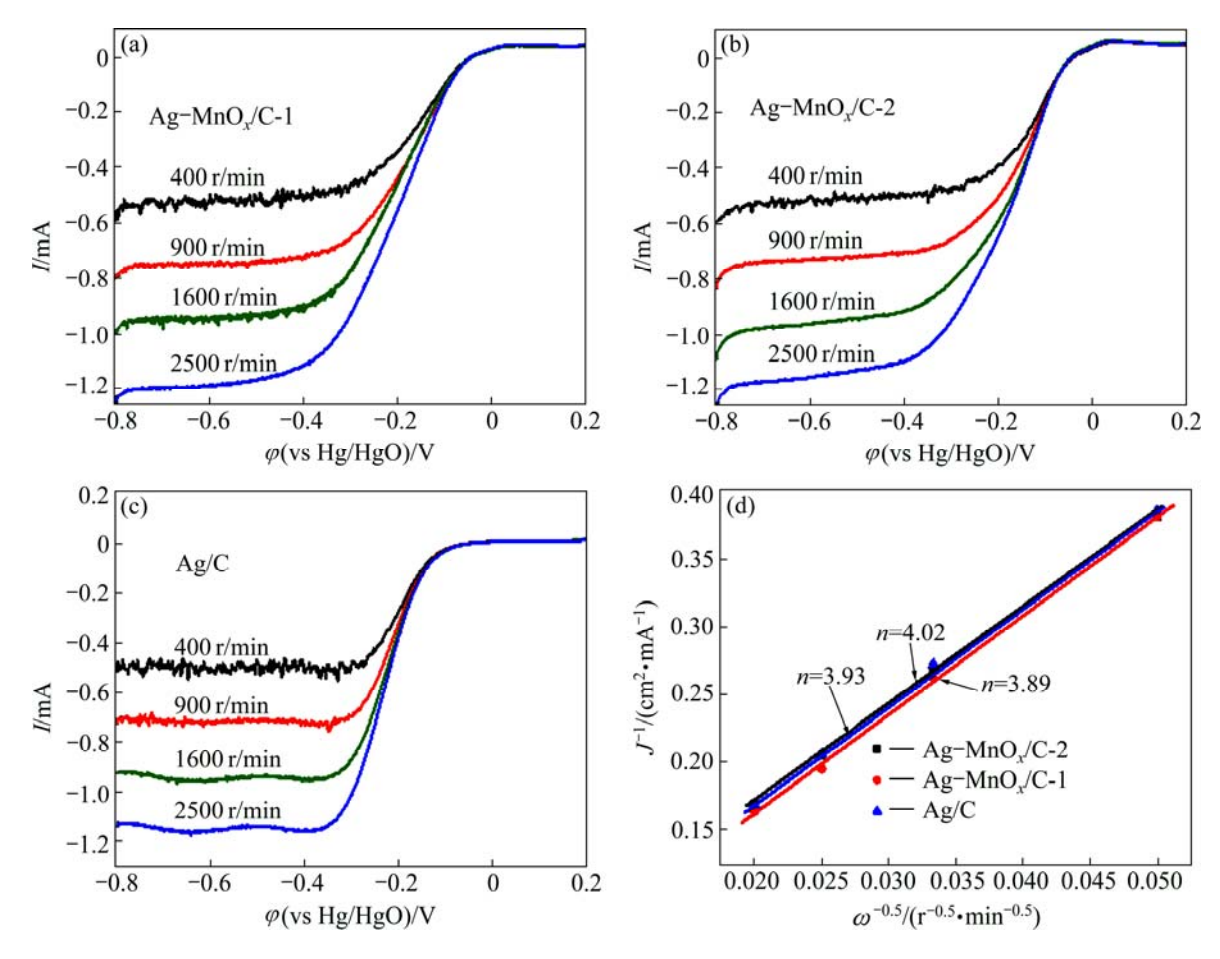


**Fig. 7** LSV curves of catalysts Ag-MnO<sub>x</sub>/C-1 (a), Ag-MnO<sub>x</sub>/C-2 (b) and Ag/C (c) at different rotation rates in O<sub>2</sub>-saturated 0.1 mol/L NaOH solution and Koutecky-Levich plots of ORR on different catalysts (d) (Scanning rate: 0.01 V/s; electrode area: 0.196 cm<sup>2</sup>)

To further verify the ORR selectivity on the composites, the RRDE measurements were done to detect the  $HO_2^-$  formation. The RRDE polarization curves of the catalysts with the rotation rate of 1600 r/min in O<sub>2</sub>-saturated 0.1 mol/L NaOH solution are shown in Fig. 8 which take on the same characteristics as that shown in Fig. 6. The correlations between the ring currents, which indicate the formation of HO2-, and the disk potentials are presented in Fig. 8(a). It can be seen that the HO<sub>2</sub> output on the Ag-MnO<sub>x</sub>/C-2 is much lower than those observed on the Ag-MnO<sub>x</sub>/C-1 and Ag/C when the potential is lower than -0.30 V. The electron transfer numbers and the HO<sub>2</sub><sup>-</sup> productions are plotted as functions of the disk potentials and shown in Fig. 8(c) and Fig. 8(d), respectively. It can be observed that during the ORR process, the HO<sub>2</sub> production on the Ag-MnO<sub>x</sub>/C-2 is obviously lower than that on the Ag-MnO<sub>x</sub>/C-1. At the potential of -0.60 V, HO<sub>2</sub> production is only 5.46%, much lower than those on the  $Ag-MnO_x/C-1$  (15.26%) and Ag/C (16.10%), and the corresponding electron transfer number is 3.90, higher than those on the  $Ag-MnO_x/C-1$  (3.70) and Ag/C (3.68).

To compare the intrinsic catalytic activities, the ORR kinetic currents (calculated by  $J_k = J \times J_{lim}/(J_{lim} - J)$ ) normalized to the geometric surface area and the mass of silver derived from Fig. 8(b) are shown in Figs. 9(a) and (b). For the Ag-MnO<sub>x</sub>/C composites, the Tafel slopes could be divided into two parts, about -55 and -120 mV/dec at low and high overpotentials, respectively. The comparable values of Tafel slopes for the Ag-MnO<sub>x</sub>/C composites and Pt/C indicate that the ORR mechanism is the same, that is, the one-electron transfer is the rate-determining step at low overpotentials and the two-electron transfer reaction is the rate- determining step at the higher overpotentials [16]. The Tafel slopes for the Ag/C are about -60 and -90 mV/dec at low and high overpotentials, respectively. At the potential of -0.10 V, the ORR kinetic current density normalized to obtained the geometric surface area on Ag-MnO<sub>x</sub>/C-2 composite is 0.92 mA/cm<sup>2</sup>, much higher than those observed on the Ag-MnO<sub>x</sub>/C-1 (0.56 mA/cm<sup>2</sup>) and Ag/C (0.12 mA/cm<sup>2</sup>). Meanwhile, the corresponding specific mass kinetic current on the Ag-MnO<sub>x</sub>/C-2 composite is 46 mA/µg, which is 23 times that on the Ag/C (2 mA/ $\mu$ g).

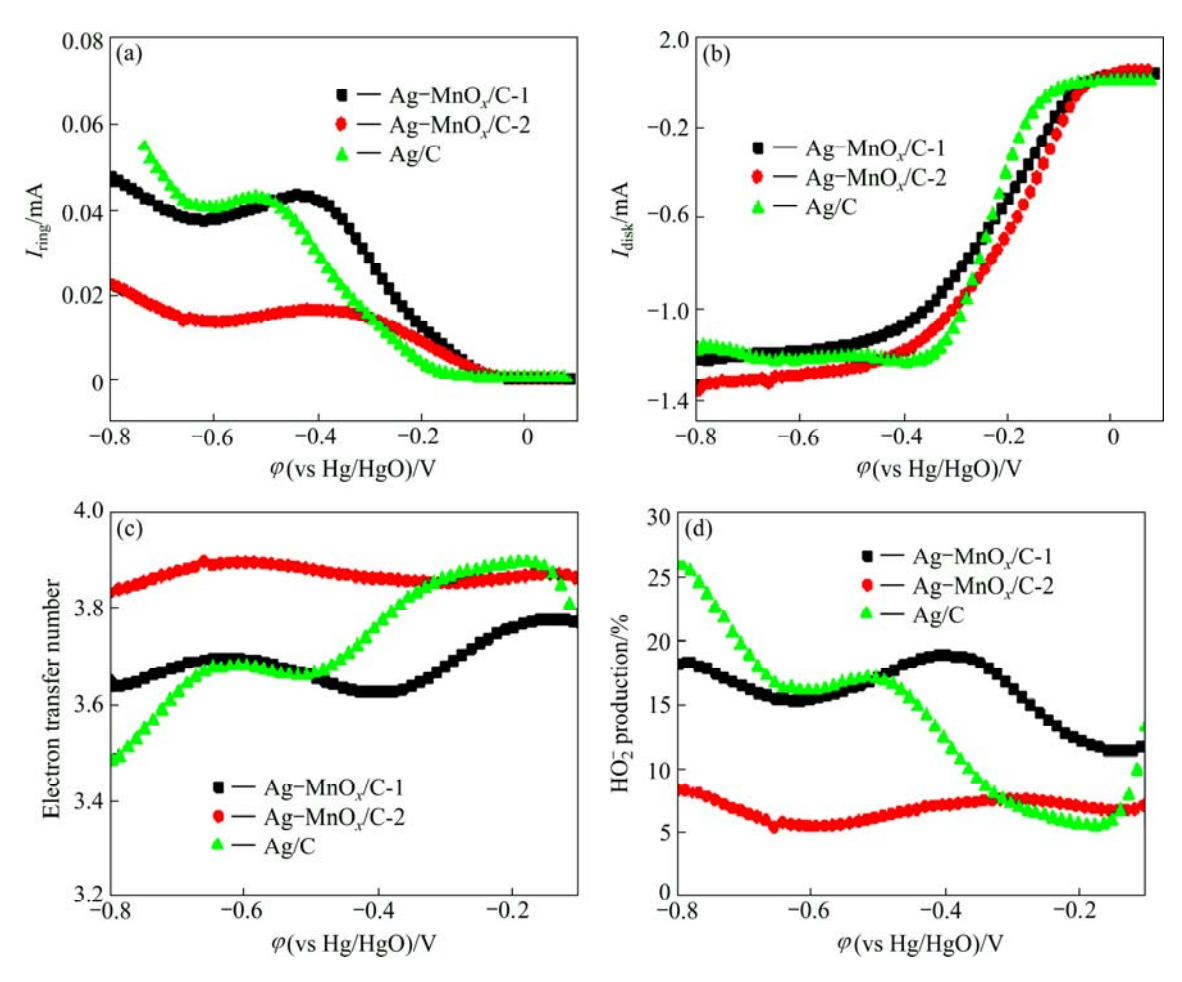


**Fig. 8** Ring currents (a), disk currents (b), electron transfer numbers (c) and  $HO_2^-$  productions (d) during RRDE measurements for Ag-MnO<sub>x</sub>/C and Ag/C composites in O<sub>2</sub>-saturated 0.1 mol/L NaOH solution at room temperature (Scanning rate: 0.01 V/s; rotation rate: 1600 r/min; electrode area: 0.255 cm<sup>2</sup>)

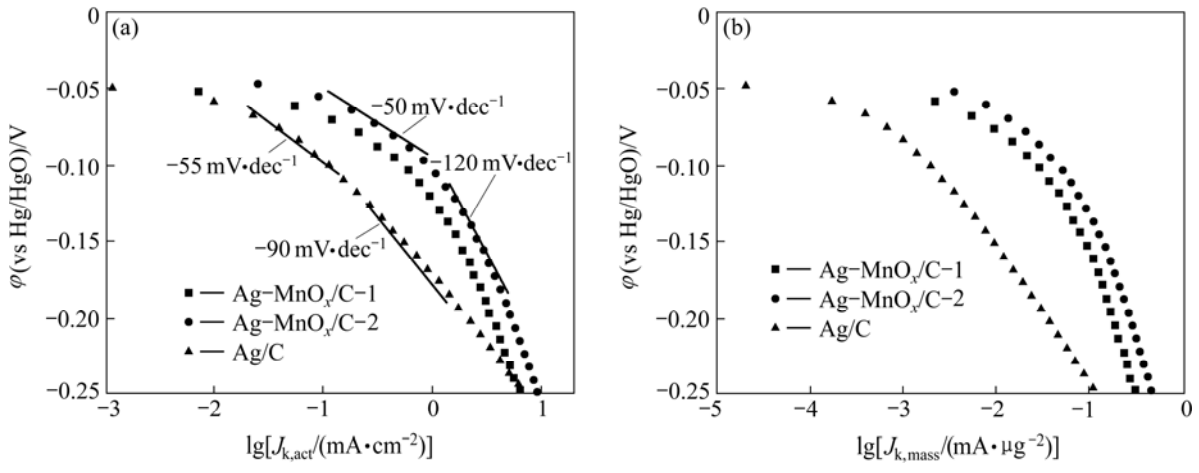


**Fig. 9** Tafel plots of ORRs on Ag–MnO<sub>x</sub>/C and Ag/C composites derived from Fig. 8(b): (a) Current normalized to geometric surface; (b) Current normalized to mass of noble metal Ag

#### 3.5 Performance of zinc-air battery

The polarization curves of the zinc–air batteries with the  $Ag-MnO_x/C$  and Ag/C as the cathode catalysts are presented in Fig. 10. When the discharge current density is  $100 \text{ mA/cm}^2$ , the voltages of the cells with the

catalysts of Ag-MnO<sub>x</sub>/C-1, Ag-MnO<sub>x</sub>/C-2 and Ag/C are about 0.87, 0.92 and 0.83 V, respectively. The peak power density reaches 117 mW/cm<sup>2</sup> for the cell based on the Ag-MnO<sub>x</sub>/C-2 air cathode, much higher than those with Ag-MnO<sub>x</sub>/C-1 (103 mW/cm<sup>2</sup>) and Ag/C

 $(90 \text{ mW/cm}^2)$  cathode catalysts, respectively. The better performance of battery based on the Ag-MnO<sub>x</sub>/C-2 catalyst shows that the composite is a promising candidate as the catalyst for the air electrode in alkaline media.

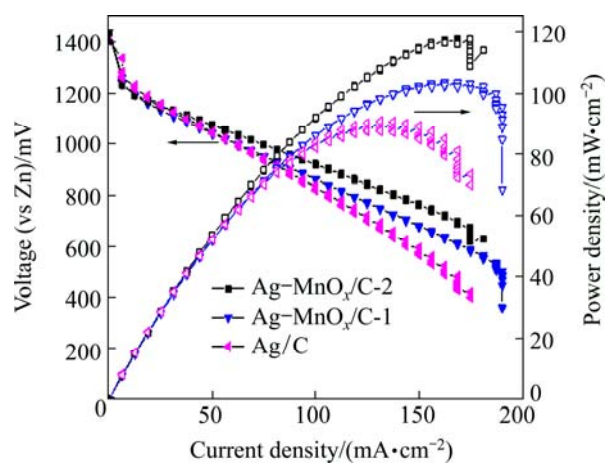


Fig. 10 Polarization curves of zinc—air single cells made up of different air electrodes

# **4 Conclusions**

- 1) Different preparation routes of  $Ag-MnO_x/C$  make no noticeable difference on the valence state of Mn. The main silver species of the composites is  $Ag_2O$ .
- 2) More Ag and Mn species present on the surface of the Ag–MnO $_x$ /C-2 composite, which contributes to its superior ORR activity. The electron transfer number involved in the ORR on the Ag–MnO $_x$ /C-2 composite is about 4, higher than those on the samples of Ag–MnO $_x$ /C-1 and Ag/C. The specific mass kinetic current on the Ag–MnO $_x$ /C-2 composite at the potential of –0.60 V is 46 mA/ $\mu$ g, which is 23 times that on the Ag/C.
- 3) The peak power density of zinc–air battery with the  $Ag-MnO_x/C-2$  air electrode reaches 117 mW/cm<sup>2</sup>, which is much higher than those with the  $Ag-MnO_x/C-1$  and Ag/C as the cathode catalysts.

# References

- ZHENG N, LIU Y, WANG Y. Methanol-tolerant carbon supported phthalocyanine-platinum nanocomposite catalytic cathode [J]. Chemical Journal of Chinese University, 2011, 32(3): 748–752.
- [2] YI Qing-feng, XIAO Xing-zhong, LIU Yun-qing. Hydrothermal synthesis of titanium-supported nanoporous palladium-copper electrocatalysts for formic acid oxidation and oxygen reduction reaction [J]. Transactions of Nonferrous Metals Society of China, 2013, 23:1184–1190.
- [3] WANG Wen-ming, LI Xiao-wei, ZOU Zhi-qing, YUAN Ting, DU Chong, XIA Bao-jia, YANG Hui. Preparation and electrocatalysis of carbon-supported Pd-Co-Au ternary alloy nanoparticles [J]. The Chinese Journal of Nonferrous Metals, 2008, 18(11): 2044–2049. (in Chinese)

- [4] YAN Xiang-hui, ZHANG Gui-rong, XU Bo-qing. Performance of polyaniline- derived Fe-N-C catalysts for oxygen reduction reaction in alkaline electrolyte [J]. Chinese Journal of Catalysis, 2013, 34: 1992–1997. (in Chinese)
- [5] GUO J, HSU A, CHU D, CHEN R. Improving oxygen reduction reaction activities on carbon-supported Ag nanoparticles in alkaline solutions [J]. The Journal of Physical Chemistry C, 2010, 114: 4324–4330.
- [6] XU X, TAN C, LIU H, WANG F, LI Z, LIU J, JI J. Carbon black supported ultra-high loading silver nanoparticle catalyst and its enhanced electrocatalytic activity towards oxygen reduction reaction in alkaline medium [J]. Journal of Electroanalytical Chemistry, 2013, 696: 9-14
- [7] LIM E J, CHOI S M, SEO M H, KIM Y, LEE S, KIM W B. Highly dispersed Ag nanoparticles on nanosheets of reduced graphene oxide for oxygen reduction reaction in alkaline media [J]. Electrochemistry Communication, 2013, 28: 100–103.
- [8] ZHANG Dong, ZHANG Cun-zhong, MU Dao-bing, WU Bo-rong, WU Feng. A review of Ag-based catalysts for oxygen reduction reaction [J]. Acta Chimica Sinica, 2013, 71: 1101–1110. (in Chinese)
- [9] LU Y, CHEN W. Size effect of silver nanoclusters on their catalytic activity for oxygen electro-reduction [J]. Journal of Power Sources, 2012, 197: 107–110.
- [10] LU Y, WANG Y, CHEN W. Silver nanorods for oxygen reduction: Strong effects of protecting ligand on the electrocatalytic activity [J]. Journal of Power Sources, 2011, 196: 3033–3038.
- [11] LIMA F H B, de CASTRO J R F, TICIANELLI E A. Silver-cobalt bimetallic particles for oxygen reduction in alkaline media [J]. Journal of Power Sources, 2006, 161: 806–812.
- [12] KOSTOWSKYJ M A, KIRK D W, THORPE S J. Ag and Ag-Mn nanowire catalysts for alkaline fuel cells [J]. International Journal of Hydrogen Energy, 2010, 35: 5666-5672.
- [13] HU F P, ZHANG X G, XIAO F, ZHANG J L. Oxygen reduction on Ag-MnO<sub>2</sub>/SWNT and Ag-MnO<sub>2</sub>/AB electrodes [J]. Carbon, 2005, 43: 2931-2936.
- [14] LEE C L, SYU C M, HUANG C H, CHIOU H P, CHAO Y J, YANG C C. Cornered silver and silver-platinum nanodisks: Preparation and promising activity for alkaline oxygen reduction catalysis [J]. Applied Catalysis B: Environmental, 2013, 132–133: 229–236
- [15] JIANG L, HSU A, CHU D, CHEN R. A highly active Pd coated Ag electrocatalyst for oxygen reduction reactions in alkaline media [J]. Electrochimica Acta, 2010, 55: 4506–4511.
- [16] TANG Q, JIANG L, QI J, JIANG Q, WANG S, SUN G. One step synthesis of carbon-supported Ag/Mn<sub>y</sub>O<sub>x</sub> composites for oxygen reduction reaction in alkaline media [J]. Applied Catalysis B: Environmental, 2011, 104: 337–345.
- [17] WU Q, JIANG L, TANG Q, LIU J, WANG S, SUN G. Activity and stability of the Ni(OH)<sub>2</sub>-MnO<sub>x</sub>/C composite for oxygen reduction reaction in alkaline solution [J]. Electrochimica Acta, 2013, 91: 314-322
- [18] ROMAND R, ROUBIN M, DELOUME J P. X-ray photoelectron emission studies of mixed selenides AgGaSe<sub>2</sub> and Ag<sub>9</sub>GaSe<sub>6</sub> [J]. Journal of Solid State Chemistry, 1978, 25: 59–64.
- [19] HUANG C C, KHU N H, YEH C S. The characteristics of sub 10 nm manganese oxide T1 contrast agents of different nanostructured morphologies [J]. Biomaterials, 2010, 31: 4073–4078.
- [20] LIMA F H B, CALEGARO M L, TICIANELLI E A. Electrocatalytic activity of manganese oxides prepared by thermal decomposition for oxygen reduction [J]. Electrochimica Acta, 2007, 52: 3732–3738.
- [21] YU L, PAN X, CAO X, HU P, BAO X. Oxygen reduction reaction mechanism on nitrogen-doped graphene: A density functional theory study [J]. Journal of Catalysis, 2011, 282: 183–190.
- [22] BARD A J, FAULKNER L R. Electrochemical methods [M]. New Delhi: Wiley, 2006.

# 制备路线对碱性介质氧还原反应电催化剂 $Ag-MnO_x/C$ 催化活性的影响

伍秋美<sup>1</sup>, 阮建明<sup>1</sup>, 周忠诚<sup>1</sup>, 桑商斌<sup>2</sup>

- 1. 中南大学 粉末冶金国家重点实验室, 长沙 410083;
  - 2. 中南大学 化学化工学院,长沙 410083

摘 要:通过 X 射线衍射、X 射线光电子能谱、透射电镜、扫描电镜以及能谱分析和电化学方法考察制备路线对氧还原反应(ORR)电催化剂  $Ag-MnO_x/C$  物理性能及其催化活性的影响。结果表明:通过两步法制得的催化剂  $(Ag-MnO_x/C-2)$ 的表面 Ag 和 Mn 含量比一步法制备样品 $(Ag-MnO_x/C-1)$ 的高,这使得  $Ag-MnO_x/C-2$  具有更高的催化活性。 $Ag-MnO_x/C-2$  表面 ORR 的电子转移数高于  $Ag-MnO_x/C-1$  的电子转移数,且在-0.60 V(相对于 Hg/HgO) 处的比质量动力学电流为 46  $mA/\mu g$ ,为 Ag/C 的 23 倍。以  $Ag-MnO_x/C-2$  为阴极催化剂组装的锌—空气电池的最高能量密度高达 117  $mW/cm^2$ 。

关键词:银;氧化锰;氧还原反应;锌-空气电池;电催化剂;燃料电池

(Edited by Yun-bin HE)